

The effects of a revised ${}^7\text{Be}$ e^- -capture rate on solar neutrino fluxes

D. Vescovi^{1,2}, L. Piersanti^{3,2}, S. Cristallo^{3,2}, M. Busso^{4,2}, F. Vissani⁵, S. Palmerini^{4,2}, S. Simonucci^{6,2}, and S. Taioli^{7,8}

¹ Gran Sasso Science Institute, Viale Francesco Crispi, 7, 67100 L'Aquila, Italy
e-mail: diego.vescovi@gssi.it

² INFN, Section of Perugia, Via A. Pascoli snc, 06123 Perugia, Italy

³ INAF, Observatory of Abruzzo, Via Mentore Maggini snc, 64100 Teramo, Italy

⁴ University of Perugia, Department of Physics and Geology, Via A. Pascoli snc, 06123 Perugia, Italy

⁵ INFN, Laboratori Nazionali del Gran Sasso, Via G. Acitelli, 22, Assergi, L'Aquila, Italy

⁶ Division of physics School of Science and Technology Università di Camerino, Italy

⁷ Faculty of Mathematics and Physics, Charles University, Prague, Czech Republic

⁸ European Centre for Theoretical Studies in Nuclear Physics and Related Areas (ECT*-FBK) and Trento Institute for Fundamental Physics and Applications (TIFPA-INFN), Trento, Italy

Received ; accepted

ABSTRACT

Context. The electron-capture rate on ${}^7\text{Be}$ is the main production channel for ${}^7\text{Li}$ in several astrophysical environments. Theoretical evaluations have to account for not only the nuclear interaction, but also the processes in the plasma where ${}^7\text{Be}$ ions and electrons interact. In the past decades several estimates were presented, pointing out that the theoretical uncertainty in the rate is in general of few percents.

Aims. In the framework of fundamental solar physics, we consider here a recent evaluation for the ${}^7\text{Be}+e^-$ rate, not used up to now in the estimate of neutrino fluxes.

Methods. We analysed the effects of the new assumptions on Standard Solar Models (SSMs) and compared the results obtained by adopting the revised ${}^7\text{Be}+e^-$ rate to those obtained by the one reported in a widely used compilation of reaction rates (ADE11).

Results. We found that new SSMs yield a maximum difference in the efficiency of the ${}^7\text{Be}$ channel of about -4% with respect to what is obtained with the previously adopted rate. This fact affects the production of neutrinos from ${}^8\text{B}$, increasing the relative flux up to a maximum of 2.7%. Negligible variations are found for the physical and chemical properties of the computed solar models.

Conclusions. The agreement with the SNO measurements of the neutral current component of the ${}^8\text{B}$ neutrino flux is improved.

Key words. Neutrinos – Nuclear reactions, nucleosynthesis, abundances – Sun: abundances – Sun: helioseismology – Sun: interior

1. Introduction

Solar models and their comparisons with observations are a powerful tool for probing the solar interiors with high accuracy, describing the trend of the sound speed and predicting how neutrinos are distributed among the various channels (see e.g. Bahcall et al. 2001, for a review).

Solar neutrino measurements, in particular those from the ${}^8\text{B}$ channel (Aharmim et al. 2013; Abe et al. 2016) yielded information on fundamental neutrino properties; nowadays these properties are measured with an increasing accuracy and detailed knowledge of neutrino fluxes maintains its importance also for this aim.

Very recently the Borexino collaboration presented the first global analysis of three individual neutrino components of the proton-proton (pp) chain, namely pp, ${}^7\text{Be}$ and pep neutrinos, putting also an upper limit to those from CNO, over an energy range from 0.19 MeV to 2.93 MeV (Agostini et al. 2018).

These new data on neutrino fluxes can be used to improve our knowledge of the solar interiors (Vinyoles et al. 2017), which is still beset with problems; among them, of special relevance are those raised by the compilations of solar abundances based on 3D atmospheric models (Asplund 2005), which lead to disagreements with the measured sound speed (Bahcall et al. 2005b).

Standard solar model predictions for neutrino fluxes are then very sensitive to the reaction rates adopted, obviously including

electron-captures in the plasma (which are also of great importance for several other astrophysical problems). The electron-capture rate on ${}^7\text{Be}$ itself is strongly dependent on the density and temperature distribution in the stellar structure (Simonucci et al. 2013); in solar conditions, in particular, this destruction channel of ${}^7\text{Be}$ dominates over proton captures (Adelberger et al. 1998). From this latter branching, through ${}^8\text{B}$ -decays, further neutrinos are emitted and can be detected by experiments like Super-Kamiokande, SNO and KamLand. The observed flux of ${}^8\text{B}$ neutrinos is expected to be inversely proportional to the electron-capture rate on ${}^7\text{Be}$, being the counting rate in experiments determined by the number of proton-capture reactions occurring per unit of time (Bahcall & Moeller 1969). Despite many different estimates presented (Bahcall 1962; Bahcall & Moeller 1969; Johnson et al. 1992; Gruzinov & Bahcall 1997), the accuracy in our knowledge of the relative importance of these two channels is not yet satisfactory and improvements have been limited over the years.

In this work we make a step forward by using a new estimate of the electron-capture rate on ${}^7\text{Be}$ (Simonucci et al. 2013, hereafter STPB13) to compute SSMs. The results are then compared with those obtained by the widely used rate by Adelberger et al. (2011) (hereafter ADE11), focusing our attention on the solar neutrino fluxes. We make use of a tabulated version of the decay rate by STPB13. The aforementioned table, available at

the CDS, contains the following information. Column 1 lists the density over the mean molecular weight for electrons in units of g cm^{-3} , Column 2 gives the temperature in units of K and Column 3 provides the value of the electron-capture rate in units of s^{-1} . All the quantities are expressed in logarithmic scale. We also present an analytical approximation to it (see section 3). Our work is organized as follows. In Section 2 the main features of the adopted stellar evolutionary code and of SSMs are described. Section 3 illustrates the calculation of the electron-capture rate on ${}^7\text{Be}$ and presents a comparison with the previous estimate. In Section 4 we analyze the main characteristics of the ensuing SSM, while in Section 5 the impact of the adopted rate on neutrinos from the ${}^8\text{B}$ channel is discussed. We summarize our results in Section 6.

2. The Standard Solar Model

A SSM represents the mathematical way of fitting the present-day Sun status, provided some boundary conditions as luminosity, radius, mass and composition are available. Other important features such as temperature, pressure, sound-speed profiles, solar photospheric abundances and neutrino fluxes can then be predicted. Each of these quantities strictly depends on the nuclear reactions at work in the Sun's interiors, whose main outcome is helium production by hydrogen burning. This occurs through the pp-chain ($\sim 99\%$) and, to a much lesser extent, through the CN-cycle ($\sim 1\%$). Although the latter is not very important for the energy production in our Sun, it is relevant for the details of the neutrino production and as a test of the correctness of the predictions. Other ingredients of the input physics, such as equation of state (EoS), opacity, chemical composition, etc. are also crucial to predict the solar quantities mentioned above.

The essentials of a SSM include the full evolution of a $1 M_{\odot}$ star from the pre-main sequence to the present solar age $t_{\odot} = 4.566$ Gyr, usually by considering that mass-loss is negligible. In addition, a SSM is required to reproduce, once the presolar composition is fixed, the present-day solar mass M_{\odot} , age, radius R_{\odot} , and luminosity L_{\odot} as well as the observed metal-to-hydrogen ratio $(Z/X)_{\odot}$ at the surface of the Sun. In order to do this, in our models we calibrated accordingly, with an iterative procedure, the initial helium and the metal mass fractions Y_{ini} and Z_{ini} , respectively) as well as the mixing-length parameter (α_{MLT}). Our solar models have been calculated with the FUNS stellar evolutionary code (Straniero et al. 2006; Piersanti et al. 2007; Cristallo et al. 2011). All the models assume a present solar luminosity of $L_{\odot} = 3.8418 \times 10^{33}$ erg s^{-1} , a present solar radius $R_{\odot} = 6.9598 \times 10^{10}$ cm and a solar mass $M_{\odot} = 1.989 \times 10^{33}$ g (Allen 1963; Bahcall et al. 2005a).

The input physics is basically the same adopted by Piersanti et al. (2007), but includes a few recent updates as listed below. We adopted the nuclear reaction rates presented in Table 1, except for the case of the ${}^7\text{Be}$ electron-captures, for which we used either the rate suggested by Adelberger et al. (2011) or the one computed by Simonucci et al. (2013). Concerning the mean energy loss in the individual branches of neutrino production, we used the experimental values suggested by Vissani (2018) (see their Table 2). For electron screening effects in the solar plasma we adopted the Salpeter formula for the weak-screening, as recommended by Gruzinov & Bahcall (1998) and Bahcall et al. (2002). The EoS is the same as the one described by Straniero (1988) for fully ionized matter, in the form updated by Prada Moroni & Straniero (2002) for $\log T$ [K] ≥ 6.0 and a Saha equation for $\log T$ [K] < 6.0 . Atomic diffusion has been included, taking into account the effects of gravitational settling and ther-

mal diffusion, by inverting the coupled set of Burgers equations (Thoul et al. 1994; Piersanti et al. 2007). For radiative opacities, we used the OPAL tables (Iglesias & Rogers 1996) for high temperatures ($\log T$ [K] ≥ 4.0) and the Ferguson et al. (2005) molecular opacities for low temperatures ($\log T$ [K] < 4.0), corresponding to the scaled-solar composition given either by Grevesse & Sauval (1998) or by Palme et al. (2014) (hereafter GS98 and PLJ14, respectively). Different choices of $(Z/X)_{\odot}$ correspond to different metal distributions in the solar structure, which, in their turn, change the calculated depth of the convective zone. Indeed, it was pointed out that SSMs with low metal abundances (i.e. with low $(Z/X)_{\odot}$ values) disagree with the helioseismologically measured sound speed, the depth of the convective zone, and the surface helium abundance (see e.g. Bahcall et al. 2004). Solving this disagreement, known as the ‘‘solar abundance problem’’, is an issue not related to ${}^7\text{Be}$ decay and is therefore beyond the scope of this work. Here we show that the effects of using the new rate are independent from the solar mixture assumed and can be stated in a quite general way.

Finally, we have to mention that all the analyses presented in the various cases of this work have been performed by keeping all the physical parameters fixed, except for the ${}^7\text{Be}$ electron-capture rate, to evaluate the specific role of this rate and to minimize the effects related to other inputs. The results obtained with the updated estimate of the ${}^7\text{Be}$ electron-capture rate given by STPB13 have been compared with those obtained with the evaluation given by ADE11 for the two mentioned stellar choices of the chemical composition. In principle, different assumptions for the composition, i.e. for the metal abundances, may lead to differences in the solar core temperature, hence also in the solar structure and in neutrino fluxes: see Section 4 for a quantitative discussion.

3. Electron-capture on ${}^7\text{Be}$

The deep stellar interiors are characterized by high densities and high temperatures. This implies that atoms are almost completely ionized; therefore, when describing the stellar core matter, it is necessary to apply the methods of plasma physics. The radioactive decay of a particular radioisotope (and its mean lifetime τ) is strongly dependent, in such plasma conditions, on the density ρ and the temperature T of the plasma itself. In short, in order to provide an estimate of decay rates in stellar conditions one has to rely on accurate models for the plasma.

Many contributions, developed between the 60's and the 80's, considered a ionized plasma, whose degree of ionization is described through the Saha equation. Free electrons, acting as a screen inside the Debye radius, are treated as a Maxwellian gas (Takahashi & Yokoi 1987). Concerning the specific case of ${}^7\text{Be}$ electron-captures, the first detailed calculation from continuum states was done by Bahcall (1962). Subsequently, estimates of the bound-electron contributions were also made (Iben et al. 1967; Bahcall & Moeller 1969; Bahcall 1994). A recommended resulting rate, based on all these calculations, was proposed by Adelberger et al. (1998) and Adelberger et al. (2011). More general treatments have also been developed over the years (Gruzinov & Bahcall 1997; Brown & Sawyer 1997; Sawyer 2011), but always referring to solar core conditions and maintaining an approach resembling the Born-Oppenheimer (BO) one. In addition to this, it was recognized that the major uncertainty affecting the decay rate arises from possible deviations from a pure Debye screening. Indeed, Johnson et al. (1992) estimated these possible corrections to the Debye-Hückel (DB) approximation by means of self-consistent thermal Hartree calculations, concluding that

Table 1. Major reaction rates included in the Standard Solar Models presented in this paper.

Reaction	Reference
${}^1\text{H}(p, \beta^+ \nu_e){}^2\text{H}$	1
${}^1\text{H}(e^- p, \nu_e){}^2\text{H}$	2
${}^2\text{H}(p, \gamma){}^3\text{He}$	2
${}^3\text{He}(p, \beta^+ \nu_e){}^4\text{He}$	2
${}^3\text{He}({}^3\text{He}, \alpha){}^2\text{H}$	2
${}^3\text{He}(\alpha, \gamma){}^7\text{Be}$	2
${}^7\text{Li}(p, \alpha){}^4\text{He}$	3
${}^7\text{Be}(p, \gamma){}^8\text{B}$	4
${}^7\text{Be}(e^-, \nu_e){}^7\text{Li}$	2, 5
${}^{12}\text{C}(p, \gamma){}^{13}\text{N}$	2
${}^{13}\text{C}(p, \gamma){}^{14}\text{N}$	2
${}^{14}\text{N}(p, \gamma){}^{15}\text{O}$	6
${}^{15}\text{N}(p, \gamma){}^{16}\text{O}$	2
${}^{15}\text{N}(p, \alpha){}^{12}\text{C}$	2
${}^{16}\text{O}(p, \gamma){}^{17}\text{F}$	2
${}^{17}\text{O}(p, \gamma){}^{18}\text{F}$	7
${}^{17}\text{O}(p, \alpha){}^{14}\text{N}$	8
${}^{14}\text{C}(p, \gamma){}^{15}\text{N}$	9
${}^{18}\text{O}(p, \gamma){}^{19}\text{F}$	10
${}^{18}\text{O}(p, \alpha){}^{15}\text{N}$	11
${}^{19}\text{F}(p, \gamma){}^{20}\text{Ne}$	12
${}^{19}\text{F}(p, \alpha){}^{16}\text{O}$	13
${}^6\text{Li}(p, \gamma){}^7\text{Be}$	12
${}^6\text{Li}(p, {}^3\text{He}){}^4\text{He}$	12
${}^9\text{Be}(p, \gamma){}^{10}\text{B}$	12
${}^9\text{B}(p, \alpha){}^6\text{Li}$	14
${}^{10}\text{B}(p, \gamma){}^{11}\text{C}$	12
${}^{10}\text{B}(p, \alpha){}^7\text{Be}$	14
${}^{11}\text{B}(p, \gamma){}^{12}\text{C}$	12
${}^{11}\text{B}(p, \alpha\alpha){}^4\text{He}$	12
${}^{14}\text{C}(\beta^-, \bar{\nu}_e){}^{14}\text{N}$	15
${}^{18}\text{F}(\beta^+, \nu_e){}^{18}\text{O}$	16
${}^{18}\text{O}(\beta^-, \bar{\nu}_e){}^{18}\text{F}$	16

References. (1) Marcucci et al. (2013); (2) Adelberger et al. (2011); (3) Lamia et al. (2012); (4) Zhang et al. (2015); (5) Simonucci et al. (2013); (6) Marta et al. (2011); (7) Di Leva et al. (2014); (8) Bruno et al. (2016); (9) Iliadis et al. (2010); (10) Buckner et al. (2012); (11) La Cognata et al. (2010); (12) Angulo et al. (1999); (13) Indelicato et al. (2017); (14) Lamia et al. (2015); (15) Rauscher & Thielemann (2000); (16) Oda et al. (1994).

the proposed rate was correct within an accuracy of about 2%. In this regard, it has to be remarked that temperature at the centre of the Sun ($T \approx 15.5$ MK) is too high for electron degeneracy to set in. Hence, the classical approximation used e.g. by Bahcall to derive his rate is well founded for the solar conditions.

Quite recently Simonucci et al. (2013) developed a first-principles approach to derive the ${}^7\text{Be}$ electron-capture rate, by modeling the electron-capture as a two-body scattering process ${}^7\text{Be}-e^-$. To this aim, the e^- -capture process is assumed to be proportional to the electronic density at the nucleus $\rho_e(0)$, which is screened and modified by the presence of the surrounding particles. We notice in passing that the DB approximation used by Bahcall represents the high-temperature classical limit of the approach developed by Simonucci et al. (2013), which provides the e^- -capture rate on ${}^7\text{Be}$ over a range of plasma densities and

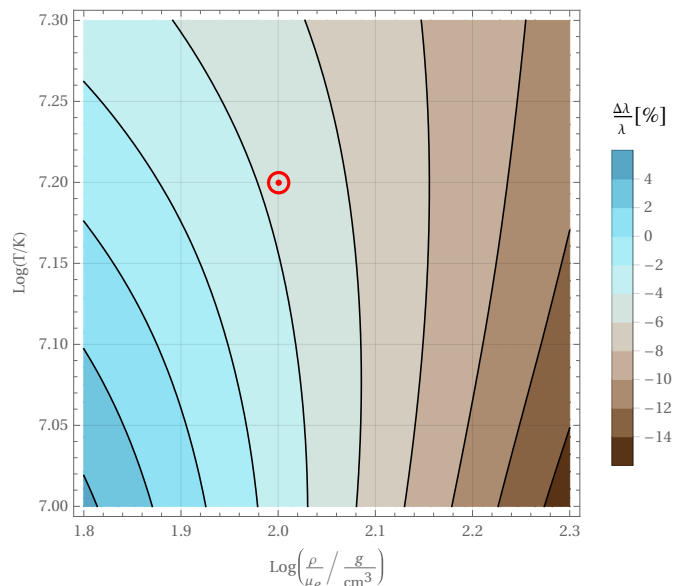


Fig. 1. The fractional variation of the ${}^7\text{Be}$ electron-capture rate, $\Delta\lambda/\lambda$ [%] = $100 \cdot (R_{\text{STPB13}} - R_{\text{ADE11}})/R_{\text{ADE11}}$, as a function of ρ/μ_e and T , adopting the Simonucci et al. (2013) rate, as compared to the Adelberger et al. (2011) one, for the PLJ14 solar composition (see Section 2). The solar core conditions are highlighted with the common solar symbol. A color version of this figure is available in the online journal.

temperatures definitively larger than that in the solar core conditions.

In this approach, the plasma is assumed hot and is modeled as a homogeneous Fermi gas made by ${}^7\text{Be}$ atoms, surrounded by N_p protons (hydrogen nuclei) and N_e electrons, at various temperatures T and densities ρ . The motion of quantum Fermi gases is ruled by the Schrödinger equation and described in a reference frame fixed on the Be nucleus. Due to the adopted non-inertial frame, the Hamiltonian of the system contains non-inertial terms, coupling the motion of particles of the different species. As Be is definitively more massive, all these terms can be safely neglected, so that a factorization of the eigenfunctions can be performed and separable eigensolutions can be found. This procedure is reminiscent of the conditions for the adiabatic theorem, and thus it represents an “adiabatic” approximation. In this way the many-body scattering problem is reduced to a screened two-body problem, so that $\rho_e(0)$ is computed by solving a coupled Hartree-Fock (HF) self-consistent system of equations for both protons and electrons, in the electric field generated by the ${}^7\text{Be}$ nucleus located at the origin of the reference frame. The HF treatment of the Coulomb repulsion is satisfactory and accurate enough to comply with the electron correlation in stellar conditions (see Simonucci et al. 2013).

The mean lifetime, resulting from this method, is in general compatible with estimates by Bahcall (1962); Bahcall & Moeller (1969); Bahcall (1994); Adelberger et al. (1998); Adelberger et al. (2011); however, it has values that, in solar conditions, are smaller by $\sim 3 - 4\%$ with respect to those estimated in the mentioned works. Far from these conditions, the differences can be much more pronounced (see Figure 1). We refer the reader to Simonucci et al. (2013) for the details of the calculations. The total reaction rate λ for ${}^7\text{Be}(e^-, \nu_e){}^7\text{Li}$ by STPB13 can also be expressed analytically in an approximate formula, as a function of temperature, density, and composition.

An expression that agrees with an accuracy of 2% to the tabulated results for the rate λ [s⁻¹], in the region of relevance for solar physics, i.e. $35 \lesssim \rho/\mu_e$ [g cm⁻³] $\lesssim 105$ and $10 \leq T_6$ [MK] ≤ 16 , is:

$$\lambda\left(\frac{\rho}{\mu_e}, T_6\right) = \frac{\rho}{\mu_e} \frac{\kappa}{\sqrt{T_6}} \left[1 + \alpha (T_6 - 16) + \beta \frac{\rho}{\mu_e} (1 + \gamma (T_6 - 16)) \right]. \quad (1)$$

Here μ_e is the mean molecular weight per electron, T_6 is the temperature in units of 10⁶ K, and ρ is the density in units of [g cm⁻³]. Thus, the electron density is $n_e = \rho/(m_p \mu_e)$, where m_p is the proton mass. The values of the four coefficients $\kappa, \alpha, \beta, \gamma$, whose units ensure the correct dimension of Eq. (1), are reported in Table 3. We notice that a non-linear term in the density is present, while it was absent in Bahcall's calculations. In fact, this term is due to the Coulomb repulsion (electron screening) acted upon the electrons, which modifies the density close to the nucleus. Taking into account such a non-linearity requires the introduction of a higher number of polynomial terms. We recall, however, that in this work we make use of a tabulated version of the decay rate by STPB13: in fact, the adopted fine resolution allows us to compute highly accurate solar models without adding further uncertainties deriving from the use of an analytical formula. Notice that in our discussion, none of the nuclear reaction rates relevant for the standard solar model has been modified, so that expected variations are entirely due to the new approach adopted in computing ⁷Be electron-capture rate. Nevertheless, the change in the electron density, due to the formalism introduced by Simonucci et al. (2013) to describe e⁻-capture on ⁷Be might be relevant also for other charged-particle interactions, leading to a correction in the screening factor. An investigation of this possibility and the quantitative estimation of this effect deserves dedicated analyses and future work.

4. Solar Neutrino Fluxes

Stars with initial mass $M \lesssim 1.2 M_\odot$ primarily burn hydrogen through the pp-chain. The latter has three main branches, namely the ppI-, ppII-, and ppIII-cycles. The pp, ⁸B β -decay and hep reactions produce neutrino spectra with characteristic shapes and with energies from zero up to a maximum energy q . In particular, the neutrinos coming from the weak hep branch are the most energetic ones produced by the Sun ($q \leq 18.773$ MeV) and, thus, are observed in the SNO and Super-Kamiokande event distributions because they populate energy bins above the ⁸B neutrino endpoint. The electron-capture reactions $p + e^- + p$ and ⁷Be + e⁻ produce, on the contrary, emission lines, possibly broadened by thermal effects. Concerning the ⁷Be neutrinos, they form two distinct lines, corresponding to population of both the ground state (89.5%) and the first excited state (10.5%) in ⁷Li (Vissani 2018).

The ppI, ppII, and ppIII contributions to solar energy generation can be determined from measurements of the pp/pep, ⁷Be, and ⁸B neutrino fluxes. Being the relative rates very sensitive to the solar core temperature T_c , one can infer from neutrino fluxes important information about the physics of the solar interior. Nowadays the pp, ⁷Be and ⁸B fluxes are quite well known, while the measured pep neutrino flux is strongly model-dependent. In particular, it depends on the metallicity assumed for estimating the competing CNO neutrinos (Agostini et al. 2018). The solar core physics is sensitive to metallicity effects because of the free-bound/bound-free transitions in metals, which are important contributors to the opacity. This means that metallicity variations alter the solar core temperature and, in turn, the fluxes of

temperature-sensitive neutrinos, such as those from ⁸B β -decay. Heavier metals (Mg, Si, and Fe) also affect the predicted neutrino fluxes (see Bahcall et al. 1982). Even if not very abundant, they are important opacity sources at the Sun center, as they are highly ionized. Instead, in the region just below the convective zone, at temperatures of a few millions kelvins, they are small contributors to the opacity. On the contrary, abundant, lighter, volatile heavy elements (C, N, O, Ne, and Ar) are partially ionized there and significantly affect the radiative opacities. This is the origin of discrepancies between helioseismological measurements and the predictions made using solar compositions with low (Z/X), as discussed in Bahcall et al. (2005b); Bahcall & Serenelli (2005). As a matter of fact, abundance variations of different metals influence different regions in the solar interior. Moreover, different CNO abundances imply an effect also on CNO burning efficiency (and corresponding neutrino fluxes) and a minor effect on the mean molecular weight and, in turn, on the thermodynamical quantities.

The net effect is that models using the GS98 compilation of abundances exhibit higher temperatures and higher densities with respect to those using the PLJ14 one (see Table 3). On the other hand, while pp and pep fluxes are only slightly modified, ⁷Be, ⁸B, ¹³N, ¹⁵O, and ¹⁷F neutrino fluxes are rather enhanced. Their fluxes are indeed strongly dependent on the central temperature T_c , with a power law of the form $\Phi \propto T_c^m$, with $m = 10.0, 24.0, 24.4, 27.1$ and 27.8 , respectively (see Bahcall & Ulmer 1996). CNO neutrino fluxes are enhanced also due to the increased burning efficiency caused by the higher CNO abundances in the GS98 compilation. As was already mentioned, using modern solar compositions like the PLJ14 one, with low surface metal abundances, one gets solar models in disagreement with helioseismological measurements (see Bahcall et al. 2004; Basu & Antia 2004; Bahcall et al. 2005a; Serenelli et al. 2011; Haxton et al. 2013; Vinyoles et al. 2017). We have checked that the predicted sound speed profiles of our computed SSMs are in agreement with others in the literature. We found that for the PLJ14 abundance choice the prediction disagrees with the measured one (Schou et al. 1998). Instead, the choice of the older GS98 composition gives a better match.

We recall however that this work is not aimed at giving the best prediction for the total neutrino fluxes nor at probing the solar metallicity problem; rather, we want to probe the effects induced on solar neutrino fluxes by varying the ⁷Be electron-capture rate only, in the light of the mentioned evaluation by STPB13.

5. Impact of a revised ⁷Be + e⁻ on the ⁸B neutrino flux

In this section we want to evaluate the impact of using a revised rate for the ⁷Be electron-capture, computed following the approach suggested by Simonucci et al. (2013), on the ⁸B neutrino flux. While pp neutrinos originate in a wide range of the Sun, corresponding to the main energy-producing region, ⁷Be and ⁸B neutrinos are produced in a hotter and narrower zone, ranging from the solar centre to about 0.15-0.2 R_⊙. The quantities R_{STPB13} and R_{ADE11} represent the electron-capture rate given by STPB13 and by ADE11, respectively. The top panel of Fig. 2 shows the ratio between the STPB13 decay rate and ADE11's one in the production region of ⁸B neutrinos, both computed on the solar structure resulting from the ADE11 SSM, with a PLJ14 composition. As shown, there is an appreciable variation: the new rate is lower with respect to the ADE11 choice in solar

Table 2. Coefficients for the analytical approximation to the STPB13 and ADE11 electron-capture rates.

	κ	α	β	γ
this paper	5.9065×10^{-9}	-1.3614×10^{-2}	-9.2042×10^{-4}	-1.5334×10^{-1}
ADE11	5.6×10^{-9}	$+4 \times 10^{-3}$	0	0

Table 3. The main relevant quantities for the solar models adopting the ADE11 rate, as defined in the text. The models using the STPB13 rate show negligible variations for the same quantities. Here R_{CE} is the radius at the base of the convective envelope, T_c and ρ_c are the central temperature and density, α_{MLT} is the value of the mixing-length parameter. X_{ini} , Y_{ini} , Z_{ini} and $(Z/X)_{\text{ini}}$ are the initial hydrogen, helium and metal abundances by mass and the initial metal-to-hydrogen ratio, while X_{\odot} , Y_{\odot} , Z_{\odot} and $(Z/X)_{\odot}$ are the corresponding present-day photospheric values.

	GS98	PLJ14
R_{CE}/R_{\odot}	0.71628	0.72294
T_c [10^7K]	1.55031	1.54286
ρ_c [g cm^{-3}]	149.377	148.325
α_{MLT}	2.31832	2.30317
X_{ini}	0.70428	0.71092
Y_{ini}	0.27703	0.27256
Z_{ini}	0.01868	0.01653
$(Z/X)_{\text{ini}}$	0.02653	0.02325
X_{\odot}	0.73656	0.74412
Y_{\odot}	0.24656	0.24103
Z_{\odot}	0.01688	0.01485
$(Z/X)_{\odot}$	0.02292	0.01995

core conditions, meaning that the ${}^7\text{Be}$ neutrino production channel is slightly suppressed in favor of all other channels. In particular, both the solar neutrino fluxes from ${}^7\text{Be}$ and ${}^8\text{B}$, $\Phi({}^7\text{Be})$ and $\Phi({}^8\text{B})$, are proportional to the local density of ${}^7\text{Be}$ ions. The $\Phi({}^7\text{Be})$ flux depends on both the electron-capture (R_{ec}) and the proton-capture rate (R_{pc}) through:

$$\Phi({}^7\text{Be}) \propto \frac{R_{\text{ec}}}{R_{\text{ec}} + R_{\text{pc}}}, \quad (2)$$

with $R_{\text{pc}} \approx 10^{-3} R_{\text{ec}}$ (see Adelberger et al. 1998). The flux $\Phi({}^7\text{Be})$ is therefore basically independent from the rates and dependent only upon the branching ratio between the reactions ${}^3\text{He}+{}^3\text{He}$ e ${}^3\text{He}+{}^4\text{He}$. On the contrary, $\Phi({}^8\text{B})$ can be written as:

$$\Phi({}^8\text{B}) \propto \frac{R_{\text{pc}}}{R_{\text{ec}} + R_{\text{pc}}} \simeq \frac{R_{\text{pc}}}{R_{\text{ec}}}, \quad (3)$$

meaning that it is inversely proportional to the electron-capture rate R_{ec} . This means that a variation of the R_{ec} should have a linear effect on neutrino flux of ${}^8\text{B}$ and negligible effects on other channels. Indeed, the STPB13 models present exactly the same physical and chemical features of the ADE11 models (see Table 3). If we take into account neutrinos that originate in each fraction of the solar radius (Figure 2, middle panel), we thus deduce that, due to the less efficient electron-capture on ${}^7\text{Be}$ rate, the ${}^8\text{B}$ neutrino production channel becomes more efficient and so $\Phi({}^8\text{B})$ is increased. It is also possible to see that, in correspondence of a change from negative to positive values of the variations in the electron-capture rate, the neutrino flux variation shifts from positive to negative values, thus corroborating the hypothesis of linearity between the electron-capture rate on

${}^7\text{Be}$ and the ${}^8\text{B}$ neutrino flux. Furthermore, if relation (3) holds, then we see that:

$$\frac{n_{\nu}({}^8\text{B})_{\text{STPB13}}}{n_{\nu}({}^8\text{B})_{\text{ADE11}}} = \frac{\Phi({}^8\text{B})_{\text{STPB13}}}{\Phi({}^8\text{B})_{\text{ADE11}}} \simeq \frac{R_{\text{ADE11}}}{R_{\text{STPB13}}}, \quad (4)$$

or, alternatively,

$$\frac{n_{\nu}({}^8\text{B})_{\text{STPB13}}}{n_{\nu}({}^8\text{B})_{\text{ADE11}}} \frac{R_{\text{STPB13}}}{R_{\text{ADE11}}} \simeq 1, \quad (5)$$

where $n_{\nu}({}^8\text{B})$ is the number of neutrinos coming from the ${}^8\text{B}$ decay. Bottom panel of Fig. 2 shows the product in the left-hand side of relation (5). Its value is consistent with unity at the sub-per mill level, meaning that relation (3) is indeed valid and that an increase of the R_{ec} has the effect of linearly decreasing the flux of ${}^8\text{B}$ neutrinos. Finally, variations by +2.6% and +2.7% in $\Phi({}^8\text{B})$ are obtained for SSMs, using a PLJ14 or a GS98 compositions, respectively (see Table 4). The adoption of the STPB13 rate for electron-captures on ${}^7\text{Be}$ has negligible effects on all other neutrino fluxes, because it induces no variation on the physics and the chemistry of the SSM itself (see Table 3).

5.1. Comparison with Solar neutrino fluxes

At the present moment we cannot tag our predicted fluxes with well defined uncertainty estimates: we should construct Monte Carlo (MC) simulations of SSMs in order to provide statistical errors to our results (see Bahcall et al. 2006; Serenelli et al. 2011; Vinyoles et al. 2017). Still we can estimate these uncertainties starting from known literature. Concerning the predicted ${}^8\text{B}$ neutrino flux, Bahcall et al. (2006) found that the 1σ theoretical uncertainty varies from 17% to 11%, depending on the adopted composition (see their Table 15 and Figure 6). Similar but smaller values were also found by Serenelli et al. (2011) and Vinyoles et al. (2017). Then we can choose, in a conservative way, the larger value of 17% as our uncertainty on the predicted ${}^8\text{B}$ neutrino flux. Similarly we can adopt an error of 10% 1σ on the ${}^7\text{Be}$ neutrino flux, as predicted by Bahcall et al. (2006), which is the highest found in the literature. We also use, as correlation coefficient of the ${}^7\text{Be}$ - ${}^8\text{B}$ neutrino fluxes, the one given by Bahcall et al. (2006) for the GS98 composition. In this way we only give a rough, but still reliable, estimate of the uncertainties affecting our neutrino flux predictions, to be compared with the measured values.

The final joint fit to all SNO data gave a total flux of neutrino from ${}^8\text{B}$ decays in the Sun of $\Phi({}^8\text{B}) = 5.25(1 \pm 0.04) \times 10^6 \text{ cm}^{-2}\text{s}^{-1}$ (Aharmim et al. 2013). The latest results of the Borexino collaboration (Agostini et al. 2018) provided a total flux of ${}^7\text{Be}$ neutrino flux of $\Phi({}^7\text{Be}) = 4.99(1 \pm 0.03) \times 10^9 \text{ cm}^{-2}\text{s}^{-1}$. Such a value is somehow model-dependent, being obtained, from the measured rates, assuming a specific mechanism of neutrino oscillations (see Agostini et al. 2018, for details). In fact, elastic scattering measurements, like the ones performed by Borexino, are mainly sensitive to ν_e Charged-Current interactions. On the contrary, the Neutral-Current detection channel

Table 4. This table presents the predicted fluxes, in units of 10^{10} (pp), 10^9 (^7Be), 10^8 (pep, ^{13}N , ^{15}O), 10^6 (^8B , ^{17}F), and 10^3 (hep) $\text{cm}^{-2}\text{s}^{-1}$ for the reference ADE11 models, presented in Table 3, for the STPB13 models and relative differences. .

	GS98			PLJ14		
	ADE11	STPB13	relative differences	ADE11	STPB13	relative differences
$\Phi(\text{pp})$	5.99	5.99	+0.20‰	6.01	6.01	+0.01‰
$\Phi(\text{pep})$	1.42	1.42	+0.25‰	1.43	1.43	+0.01‰
$\Phi(\text{hep})$	8.09	8.09	+0.15‰	8.22	8.22	+0.01‰
$\Phi(^7\text{Be})$	4.74	4.74	+0.38‰	4.54	4.54	-0.01‰
$\Phi(^8\text{B})$	5.28	5.42	+2.70%	4.82	4.95	+2.60%
$\Phi(^{13}\text{N})$	2.82	2.82	+0.67‰	2.55	2.55	+0.06‰
$\Phi(^{15}\text{O})$	2.07	2.07	+0.71‰	1.82	1.82	+0.07‰
$\Phi(^{17}\text{F})$	5.35	5.35	+0.80‰	3.95	3.95	+0.07‰

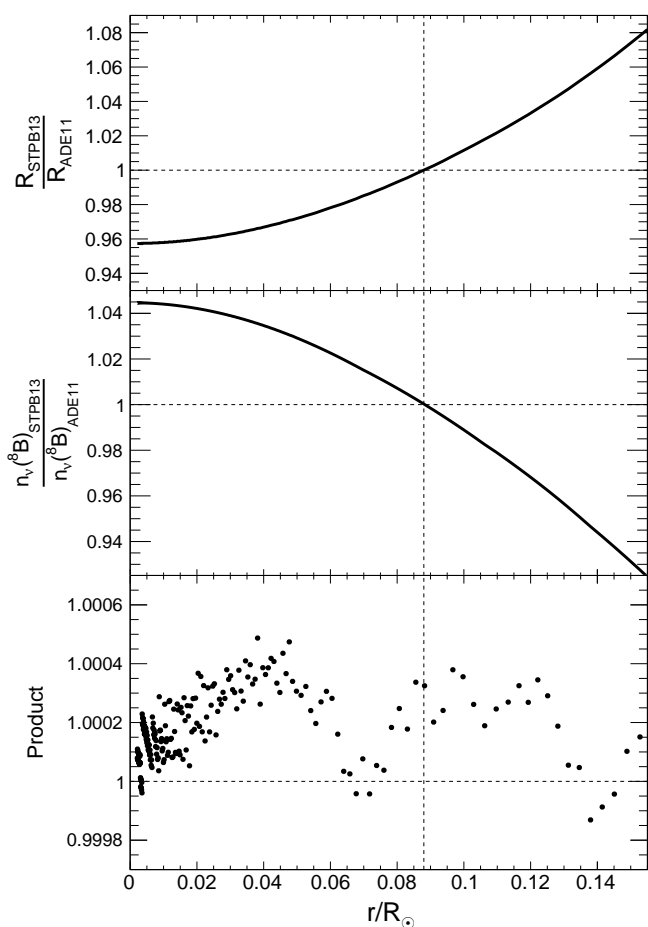


Fig. 2. Top panel shows the ratio between the STPB13 electron-capture rate and ADE11's one in the production region of ^8B neutrinos, both computed on the solar structure resulting from the ADE11 SSM, with a PLJ14 composition. Middle panel shows the ratio between the neutrinos fraction produced in STPB13 SSM and a ADE11 one, both computed with a PLJ14 composition. On the bottom panel the product $n_\nu(^8\text{B})_{\text{STPB13}} \cdot R_{\text{STPB13}} / (n_\nu(^8\text{B})_{\text{ADE11}} \cdot R_{\text{STPB13}})$ is shown; note, in comparison with the other two panels, the much finer vertical scale. The consistency of this value with the unity means that there is practically no difference in computing a SSM with the revised STPB13 rate or apply it directly on the solar structure of a ADE11 SSM.

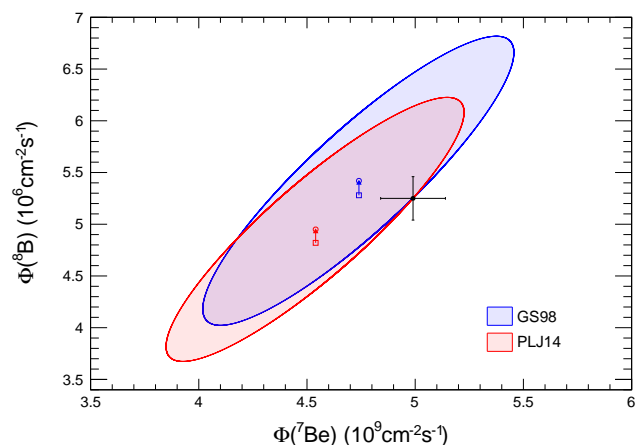


Fig. 3. $\Phi(^8\text{B})$ and $\Phi(^7\text{Be})$ fluxes compared to solar values (Aharmim et al. 2013; Agostini et al. 2018). Black dot and error bars indicate solar values, while squares and circles indicate the results obtained with the ADE11 electron-capture rate (older) and the STPB13 (current) one, respectively. Ellipses denote theoretical 1σ Confidence Level (C.L.) for 2 degrees of freedom. A color version of this figure is available in the online journal.

in SNO is sensitive to all neutrino flavours and so it is a direct model-independent observation of the ^8B solar neutrino flux. Figure 3 shows that adopting either the GS98 or the PLJ14 compositions, leads to a fair agreement with the total ^8B neutrino flux measured by the SNO neutral current experiments. The use of the revised electron-capture rate R_{STPB13} increases the old values of the predicted ^8B neutrino fluxes with respect to the measured value. The measured value of the ^8B neutrino flux is compatible with the solar model predictions for each of the two adopted solar compositions.

6. Conclusions

We have presented new SSMs for two different mixtures of solar abundances, GS98 and PLJ14. Simulations have been performed with the FUNS code suite. We used recent values for the cross sections in our nuclear reaction network. In particular, we adopt the e^- -capture rate on ^7Be provided by Simonucci et al. (2013) based on a description of the physical conditions in the solar interior more accurate than previous works (eg. ADE11) and applicable also for more general stellar environments. A tabulated version of this rate is available in the online material. The com-

parison with models computed with the ADE11 widely adopted electron-capture rate shows maximum differences of about 3-4% in solar conditions. The effects on the standard solar model calculations, along with the effects on neutrino fluxes, have been discussed. We found that variations in the Solar structure and in neutrino fluxes are negligible, except for the ${}^8\text{B}$ neutrino flux. The estimated increase is 2.6-2.7%, depending on the composition assumed. Finally, we have also shown that the solar ${}^8\text{B}$ neutrino flux is reproduced rather well, both using the GS98 and the PLJ14 abundance sets.

Acknowledgements. We warmly thank the referee, S. Degl'Innocenti, for the insightful comments and suggestions that helped us to improve the manuscript.

References

- Abe, K., Haga, Y., Hayato, Y., et al. 2016, *Phys. Rev. D*, 94, 052010
- Adelberger, E. G., Austin, S. M., Bahcall, J. N., et al. 1998, *Rev. Mod. Phys.*, 70, 1265
- Adelberger, E. G., García, A., Robertson, R. G. H., et al. 2011, *Reviews of Modern Physics*, 83, 195
- Agostini, M., Altenmüller, K., Appel, S., et al. 2018, *Nature*, 562, 505
- Aharmim, B., Ahmed, S. N., Anthony, A. E., et al. 2013, *Phys. Rev. C*, 88, 025501
- Allen, C. W. 1963, *Astrophysical quantities*
- Angulo, C., Arnould, M., Rayet, M., et al. 1999, *Nuclear Physics A*, 656, 3
- Asplund, M. 2005, *ARA&A*, 43, 481
- Bahcall, J. N. 1962, *PhRv*, 126, 1143
- Bahcall, J. N. 1994, *Phys. Rev. D*, 49, 3923
- Bahcall, J. N., Basu, S., Pinsonneault, M., & Serenelli, A. M. 2005a, *The Astrophysical Journal*, 618, 1049
- Bahcall, J. N., Brown, L. S., Gruzinov, A., & Sawyer, R. F. 2002, *A&A*, 383, 291
- Bahcall, J. N., Huebner, W. F., Lubow, S. H., Parker, P. D., & Ulrich, R. K. 1982, *Reviews of Modern Physics*, 54, 767
- Bahcall, J. N. & Moeller, C. P. 1969, *ApJ*, 155, 511
- Bahcall, J. N., Pinsonneault, M. H., & Basu, S. 2001, *ApJ*, 555, 990
- Bahcall, J. N. & Serenelli, A. M. 2005, *ApJ*, 626, 530
- Bahcall, J. N., Serenelli, A. M., & Basu, S. 2005b, *The Astrophysical Journal Letters*, 621, L85
- Bahcall, J. N., Serenelli, A. M., & Basu, S. 2006, *ApJS*, 165, 400
- Bahcall, J. N., Serenelli, A. M., & Pinsonneault, M. 2004, *ApJ*, 614, 464
- Bahcall, J. N. & Ulmer, A. 1996, *Phys. Rev. D*, 53, 4202
- Basu, S. & Antia, H. M. 2004, *The Astrophysical Journal Letters*, 606, L85
- Brown, L. S. & Sawyer, R. F. 1997, *ApJ*, 489, 968
- Bruno, C. G., Scott, D. A., Aliotta, M., et al. 2016, *Phys. Rev. Lett.*, 117, 142502
- Buckner, M. Q., Iliadis, C., Cesaratto, J. M., et al. 2012, *Phys. Rev. C*, 86, 065804
- Cristallo, S., Piersanti, L., Straniero, O., et al. 2011, *ApJS*, 197, 17
- Di Leva, A., Scott, D. A., Caciolli, A., et al. 2014, *Phys. Rev. C*, 89, 015803
- Ferguson, J. W., Alexander, D. R., Allard, F., et al. 2005, *ApJ*, 623, 585
- Grevesse, N. & Sauval, A. J. 1998, *Space Sci. Rev.*, 85, 161
- Gruzinov, A. V. & Bahcall, J. N. 1997, *The Astrophysical Journal*, 490, 437
- Gruzinov, A. V. & Bahcall, J. N. 1998, *ApJ*, 504, 996
- Haxton, W., Robertson, R. H., & Serenelli, A. M. 2013, *Annual Review of Astronomy and Astrophysics*, 51, 21
- Iben, Jr., I., Kalata, K., & Schwartz, J. 1967, *ApJ*, 150, 1001
- Iglesias, C. A. & Rogers, F. J. 1996, *ApJ*, 464, 943
- Iliadis, C., Longland, R., Champagne, A. E., Coc, A., & Fitzgerald, R. 2010, *Nuclear Physics A*, 841, 31
- Indelicato, I., La Cognata, M., Spitaleri, C., et al. 2017, *ApJ*, 845, 19
- Johnson, C. W., Kolbe, E., Koonin, S. E., & Langanke, K. 1992, *ApJ*, 392, 320
- La Cognata, M., Spitaleri, C., & Mukhamedzhanov, A. M. 2010, *ApJ*, 723, 1512
- Lamia, L., Spitaleri, C., La Cognata, M., Palmerini, S., & Pizzone, R. G. 2012, *A&A*, 541, A158
- Lamia, L., Spitaleri, C., Tognelli, E., et al. 2015, *ApJ*, 811, 99
- Marcucci, L. E., Schiavilla, R., & Viviani, M. 2013, *Physical Review Letters*, 110, 192503
- Marta, M., Formicola, A., Bemmerer, D., et al. 2011, *PhRvC*, 83, 045804
- Oda, T., Hino, M., Muto, K., Takahara, M., & Sato, K. 1994, *Atomic Data and Nuclear Data Tables*, 56, 231
- Palme, H., Lodders, K., & Jones, A. 2014, *Solar System Abundances of the Elements*, ed. A. M. Davis, 15–36
- Piersanti, L., Straniero, O., & Cristallo, S. 2007, *A&A*, 462, 1051
- Prada Moroni, P. G. & Straniero, O. 2002, *ApJ*, 581, 585
- Rauscher, T. & Thielemann, F.-K. 2000, *Atomic Data and Nuclear Data Tables*, 75, 1
- Sawyer, R. F. 2011, *PhRvC*, 83, 065804
- Schou, J., Antia, H. M., Basu, S., et al. 1998, *ApJ*, 505, 390
- Serenelli, A. M., Haxton, W. C., & Peña-Garay, C. 2011, *The Astrophysical Journal*, 743, 24
- Simonucci, S., Taioli, S., Palmerini, S., & Busso, M. 2013, *ApJ*, 764, 118
- Straniero, O. 1988, *A&AS*, 76, 157
- Straniero, O., Gallino, R., & Cristallo, S. 2006, *Nuclear Physics A*, 777, 311
- Takahashi, K. & Yokoi, K. 1987, *ADNDT*, 36, 375
- Thoul, A. A., Bahcall, J. N., & Loeb, A. 1994, *ApJ*, 421, 828
- Vinyoles, N., Serenelli, A. M., Villante, F. L., et al. 2017, *ApJ*, 835, 202
- Vissani, F. 2018, *ArXiv e-prints [arXiv:1808.01495]*
- Zhang, X., Nollett, K. M., & Phillips, D. R. 2015, *Physics Letters B*, 751, 535